mater.scichina.com link.springer.com

Published online 22 November 2021 | https://doi.org/10.1007/s40843-021-1827-x
Sci China Mater 2022, 65(4): 913–919

Breaking the energy density limit of $LiNiO_2$: Li_2NiO_3 or Li_2NiO_2?

Yining Jia[1], Yaokun Ye[1], Jiahua Liu[1], Shisheng Zheng[1], Weicheng Lin[1], Zhu Wang[1], Shunning Li[1], Feng Pan[1*] and Jiaxin Zheng[1,2*]

ABSTRACT **The development of next-generation layered oxide cathodes for high-energy-density electrical vehicle Li-ion batteries (LIBs) is an urgent topic. The existing method is achieved by continuously increasing the Ni contents of Ni-based layered oxides, but it has been limited to $LiNiO_2$. To break this limit and attain increased energy densities, a promising strategy, which involves the introduction of excess Li ions into transition metal (TM) layers to form Li-excess compounds Li_2MO_3 (M is a TM cation), has attracted enormous interest recently. However, another strategy, which has been neglected in recent years, involves the insertion of an extra layer of Li ions between the TM and original Li layers to form Li_2MO_2. In this study, typical reversible Li_2NiO_3 and 1T-Li_2NiO_2 were selected as two representative cathodes to break the limit of $LiNiO_2$, thereby availing comprehensive comparison with $LiNiO_2$ regarding their overall properties as cathodes from a theoretical perspective. Interestingly, dissimilar to the Ni^{3+}/Ni^{4+} monoelectron cationic redox associated with $LiNiO_2$, a polaronic anionic redox reaction occurs in Li_2NiO_3, while a reversible Ni^{2+}/Ni^{4+} double-electron redox reaction accompanied by insulator-metal transition occurs in Li_2NiO_2. Owing to this double-electron cationic activity, Li_2NiO_2 exhibits absolute advantages over the other two materials ($LiNiO_2$ and Li_2NiO_3) as cathodes for LIBs in terms of the capacity, energy density, electronic conductivity, and thermal stability, thus rendering it the most promising candidate for next-generation layered oxide cathodes with high energy densities to break the limit of $LiNiO_2$.**

Keywords: Li-ion battery, Li_2NiO_3 and Li_2NiO_2, double-electron redox, anionic redox, theoretical perspective

INTRODUCTION

Rechargeable Li-ion batteries (LIBs) are employed to power most recent portable electronics, as well as electrical vehicles (EVs) and grid energy storage. Accounting for the largest components (based on the weight and cost) in state-of-the-art LIB cells, cathode materials mainly determine their cell-level specific energy. Over the last decade, Ni-based layered oxides $\{Li[Ni_xMn_yCo_z]O_2$ (NMC) and $Li[Ni_{1-x-y}Co_xAl_y]O_2$ (NCA) [1,2]$\}$ have solidified their status as the most preferred cathode material for passenger EV batteries, gradually replacing cubic spinel ($LiMn_2O_4$) and olivine ($LiFePO_4$). The energy densities of layered oxides can be generally improved by continuously increasing the Ni contents; $LiNiO_2$ is the limit for this increase, thus provoking the following interesting question: is it possible to break this limit and attain higher energy density than $LiNiO_2$?

One strategy that has recently attracted enormous interest involves the introduction of excess Li ions into the transition metal (TM) layers to form Li-excess compounds, such as Li_2MO_3 (M is a TM cation) [3–5]. However, this strategy suffers from capacity fade with cycling owing to the irreversible loss of the lattice O during the anionic redox process. Another strategy, which has been neglected in recent years, involves sandwiching one layer of Li ions between the TM and original Li layers, thus obtaining a Li_2MO_2 composition. For example, Li_2CuO_2 [6], Li_2NiO_2 [7,8], Li_2CoO_2 [9], Li_2FeO_2 [9], and $Li_2Ni_xMn_yCo_zO_2$ [10] have been experimentally demonstrated as active compounds or additives in cathodes for LIB applications. Moreover, Li_2CuO_2 is a typical Li_2MO_2 material, which exhibits high theoretical capacity [6], although it is susceptible to irreversible phase transitions during cycling. Thus, the incorporation of other metal cations, such as Mn, Fe, Al, or Ni, into Li_2CuO_2 was adopted [11–16] to improve Li-ion migration and stabilize the structure. Li_2NiO_2 was employed as a cathode [7,8] or sacrificing positive additive in some commercial LIBs in which it affords overdischarge protection [17,18]. Previous studies reported that the synthesized *Immm* phase of Li_2NiO_2 (I-Li_2NiO_2) would be irreversibly transformed into the $P\bar{3}m1$ phase (1T-Li_2NiO_2) during the first cycle and that this phase would remain unchanged, following further reversible cycles [7,8]. Similar to the NMC layered cathode, the Ni cations in Li_2NiO_2 can also be replaced by other TM cations, such as Mn, Co, or Ti, which can increase the reversible capacity and cycling stability of Li_2NiO_2 [10,19], and this provoked another question: which layered oxide is more promising to break the $LiNiO_2$ limit, Li_2MO_3 or Li_2MO_2?

The phase diagram of the Li_2O–NiO–O region (Fig. 1a) revealed that Li_2NiO_3 and Li_2NiO_2 were the main phases that were identified among the diverse Ni-based lithiation TM layered oxides. Therefore, two typical reversible cathodes, Li_2NiO_3 and 1T-Li_2NiO_2, were selected as two representative materials for developing next-generation TM layered oxide cathodes to break the limit of the energy density ($LiNiO_2$) and avail comprehensive theoretical comparison with $LiNiO_2$ regarding their overall properties as cathodes. Dissimilar to the Ni^{3+}/Ni^{4+} monoelectron cationic redox in $LiNiO_2$, a polaronic anionic redox was observed in Li_2NiO_3, while a reversible Ni^{2+}/Ni^{4+} double-electron redox, which was accompanied by an

[1] School of Advanced Materials, Peking University, Shenzhen Graduate School, Shenzhen 518055, China
[2] Fujian Science & Technology Innovation Laboratory for Energy Devices of China (21C-LAB), Ningde 352100, China
* Corresponding authors (emails: zhengjx@pkusz.edu.cn (Zheng J); panfeng@pkusz.edu.cn (Pan F))

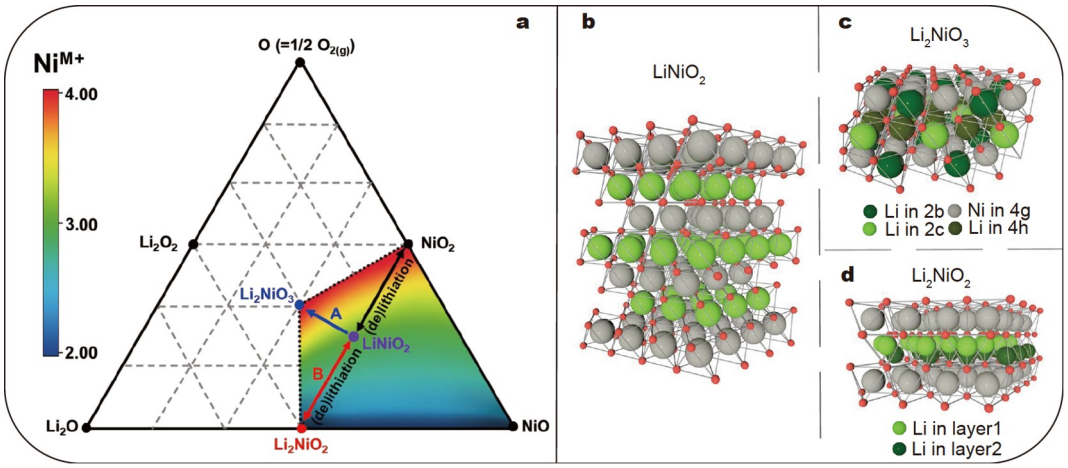

Figure 1 Pseudo phase diagrams of the Li_2O–NiO–$1/2O_2$ system and $LiNiO_2$, Li_2NiO_3, and Li_2NiO_2 crystals. (a) The corners represent typical LNO precursors; the circles indicate relevant compounds. The arrows represent the irreversible reactions, while the double arrows represent the reversible ones. The color scale denotes the Ni oxidation state. (Reproduced from Ref [22]. Copyright 2018, the German Chemical Society.) (b) $LiNiO_2$. Green: Li, red: O, silver: Ni. (c) Li_2NiO_3. Green: Li, red: O, silver: Ni. (d) Li_2NiO_2. Green: Li, red: O, silver: Ni.

insulator-metal transition, was observed in Li_2NiO_2. Owing to the double-electron cationic activity, Li_2NiO_2 was considered the most promising candidate among the three materials as cathodes for LIBs for next-generation layered oxide cathodes, which can break the $LiNiO_2$ limit, owing to its advantages in terms of the capacity, energy density, electronic conductivity, and thermal stability. We expect that these findings can avail the inspiration and basis for developing next-generation layered oxide cathodes with higher energy densities than those of $LiNiO_2$.

METHODS

Density functional theory was employed for all our calculations. The electron–core interactions were treated by the projector augmented-wave pseudopotentials with a kinetic energy cutoff of 520 eV.

The calculations were performed with the Vienna *ab initio* simulation package. Structure optimization was performed according to the generalized gradient approximation (GGA). Considering the strong onsite Coulomb repulsion among Ni-3d electrons, the Hubbard correction term, U (GGA + U) [20], was applied. This work uses an effective U value of 6.2 eV for Ni selected based on the Materials Project databases [21]. Geometry optimization was performed with no symmetry constraints, thus allowing all the atoms to relax into their most stable positions until the forces and energy were <0.015 eV $Å^{-1}$ and $<10^{-4}$ eV, respectively. Regarding the structures in which Ni ions exhibited magnetic moment, the difference between the antiferromagnetic and ferromagnetic spin orderings was considered. The difference in the energy between the spin configurations did not exceed 30 meV per Ni ion; thus, ferromagnetic spin ordering was selected.

RESULTS

Crystal and electronic structures

$LiNiO_2$ is a layered oxide containing a cubic close-packed array of O atoms [22]. It exhibits a rhombohedral structure, which is isostructural with α-$NaFeO_2$, crystallizing in the $R\bar{3}m$ space group. The octahedral interstices, which are separated by O layers, are filled by Ni and Li ions (Fig. 1b and Fig. S1a). Further, $LiNiO_2$ can be obtained *via* solid-state synthesis, sol–gel method, combustion, and coprecipitation methods [22]. Fig. 1c shows that Li_2NiO_3 is still related to the layered $LiNiO_2$ since they both exhibit layers of close-packed O ions, which separate the layers of pure Li ions from those of $[Li_{1/3}Ni_{2/3}]O_2$ containing Ni ions in honeycomb ordering [23]. The symmetry of this compound was lowered to monoclinic $C2/m$, which was isostructural with Li_2MnO_3 exhibiting the $C/2m$ space group. The structure of pristine Li_2NiO_3 exhibits two distinct octahedral sites in each layer, as follows: 4g and 2b sites in the Li/Ni layer and 4h and 2c sites in the Li layer. The Ni ions assumed the 4g position, while the Li ions occupied the 2b, 2c, and 4h sites (Fig. 1c and Fig. S1b). The synthetic procedure of Li_2NiO_3 involves a solid-state reaction between Li_2O_2 and NiO in an oxygen-rich atmosphere at high pressures to stabilize the Li ions in the Ni layers [24,25]. Fig. 1d and Fig. S1c show that 1T-Li_2NiO_2 afforded one layer of Li ions, which was incorporated into $LiNiO_2$ to obtain two-layered Li_2NiO_2 that was isostructural to Li_2VSe_2 [26]. The structure of the Li_2NiO_2 phase was refined in the $P\bar{3}m1$ space group according to the 1T phase [7]. The intercalation of additional Li ions ensured the collective transition of all the Li ions from octahedral to tetrahedral positions. The Ni ions filled the octahedral interstices between the close-packed O-planes and the Li ions between the extensively separated and alternate O layers. Thus, 1T-Li_2NiO_2 can be obtained *via* the over-lithiation of layered $LiNiO_2$ [7].

Further, the electronic structures of $LiNiO_2$, Li_2NiO_3, and Li_2NiO_2 are shown in Fig. 2. The Ni ions exhibited +3 valence states in $LiNiO_2$, and only one of its two orbitals in the e_g levels was occupied (Fig. S2); thus, the spinup e_g band was observed on the Fermi level (Fig. S3a), indicating a conducting behavior (Fig. 2a), which correlates with previous theoretical publications [27]. Conversely, the electrical measurements demonstrated that $LiNiO_2$ was a semiconductor exhibiting a small bandgap (~0.5 eV) [28]. Thus far, this difference between the theoretical calculation and experimental measurement is yet to be well understood [22] (S2 contains the detailed discussion). In Li_2NiO_3, all the electrons in the Ni-3d-e_g orbital were transferred into the O-2p orbital, after which the Ni ions exhibited +4 valence states (Fig. S2). The conduction band (CB) minimum and valence band (VB) maximum were contributed by the Ni-

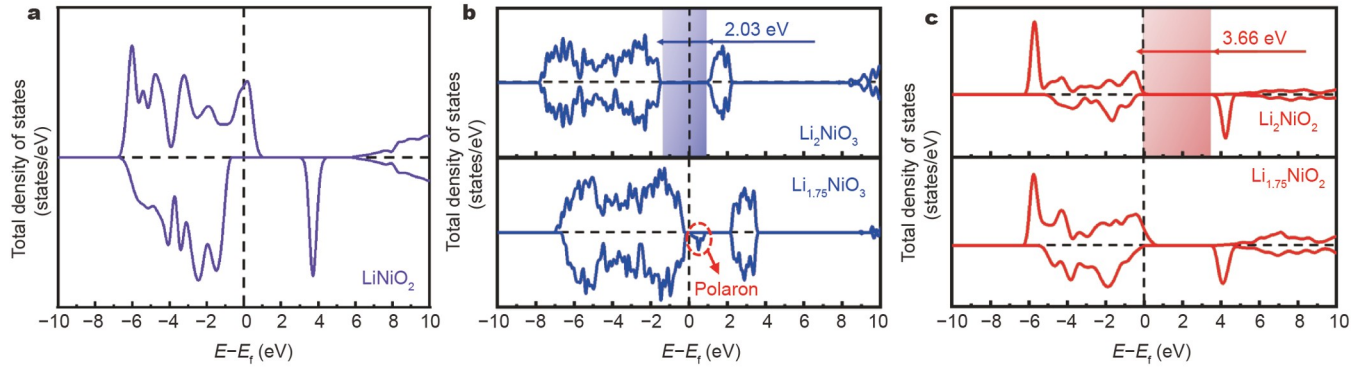

Figure 2 Electronic structures of $LiNiO_2$, Li_2NiO_3, and Li_2NiO_2. (a) Total DOS of $LiNiO_2$. (b) Total DOS of Li_2NiO_3 and $Li_{1.75}NiO_3$. (c) Total DOS of Li_2NiO_2 and $Li_{1.75}NiO_2$.

3d-e_g and Ni-3d-t_{2g} states, respectively (Fig. S3b). The total density of states (DOS) exhibited a semiconducting behavior with a bandgap of 2.03 eV (Fig. 2b). Following the partial extraction of Li ions, polaronic states appeared in the bandgap and were detrimental to the electrical conductivity [29]. This finding is consistent with the inferior electronic conductivity of Li_2MO_3 that was previously reported [30–32]. In Li_2NiO_2, two electrons were transferred from the Ni-3d-e_g orbital to the O-2p orbital, imparting Ni ions with the +2 valence state (Fig. S2). The CB minimum, as well as the highest VB maximum states, were contributed by the Ni-3d-e_g orbitals (Fig. S3c), which also exhibited a semiconductor behavior with a bandgap of 3.66 eV (Fig. 2c). Similar to $LiCoO_2$, an insulator-metal transition accompanied by slight Li-ion extraction was also observed [33], and it indicated the superior electronic conductivity of Li_2NiO_2. These results indicated that $LiNiO_2$ and Li_2NiO_2 exhibited outstanding electrical conductivities as cathodes, while Li_2NiO_3 had poor conductivity.

Charge compensation during delithiation

The charge compensation mechanisms in the three materials during delithiation were analyzed. The projected DOS (PDOS) is shown in Fig. 3. The evolution of PDOS for the partially delithiated $Li_{(1-x)}NiO_2$ (x = 0, 0.25, 0.5, and 1) is shown in Fig. 3a. It was observed that the Ni-3d PDOS above the Fermi level shifted to higher energy with hole doping induced by Ni^{4+} (the green dashed area in Fig. 3a) as x increased from 0 to 1, indicating the significant contributions from the oxidation reactions of Ni (from Ni^{3+} to Ni^{4+}). Concurrently, the magnetic moments of all the Ni cations changed from 1.427 to 0 μ_B by sequence (from x = 0 to 1), indicating the existence of the redox couple $Ni^{3+}(t_{2g}^6e_g^1)$/$Ni^{4+}(t_{2g}^6e_g^0)$ during delithiation (Table S1). Indeed, the literature reported that anionic redox had been experimentally observed in layered oxides [34,35]. In our work regarding $Li_{1-x}NiO_2$, it was observed that the magnetic moments of O were not strictly equal to zero and that the maximum magnetic moment did not exceed 0.2, indicating the slight charge transfer of the oxygen ions. Therefore, in this work, the slight anionic redox activity was neglected, whereas the cationic redox was considered the main charge compensation process in $LiNiO_2$ upon delithiation.

Considering the possible anionic redox activity in Li_2NiO_3, the hybrid functional in the form of the Heyd–Scuseria–Ernzerhof (HSE06) screened hybrid functional was applied to correct the notorious self-interaction error [36,37]. Fig. 3b shows that the O-2p behavior crossed the Fermi level upon delithiation from x = 0 up to x = 1.25, indicating that the O anion played an active role. Moreover, our results for the magnetic moments also demonstrated that with the extraction of Li up to a critical state (x = 1.25), the magnetic moments of the Ni ions remained unchanged while the magnetic moments of the O ions increased from 0 to nearly 1 μ_B, further proving that Ni ions did not participate in the redox process and that the charge, following the extraction of Li, was only compensated by the oxidation of the O ions (Table S2). When the delithiation content exceeded x = 1.25, the O-2p PDOS continued to shift to higher energy levels with additional hole doping; the magnetic moments of the O ions nearly dropped to zero (Fig. 4a and Table S2). These results demonstrated that a further extraction of Li ions (x > 1.25) triggered the O ions in the zero-valence states. Simultaneously, we noticed that some of the O–O distances had decreased to <1.4 Å (Fig. S4b), indicating the formation of O dimers [38].

For $Li_{(2-x)}NiO_2$, the Ni-3d PDOS gradually shifted to a higher level during the delithiation process (Fig. 3c), and the 3d PDOS of the oxidized Ni^{3+} and Ni^{4+} were highlighted by purple and green dashed areas, respectively, indicating the sequential oxidation of Ni^{2+}/Ni^{4+}. The magnetic moments of Ni ions also changed from 1.776 to 1.113 μ_B (from x = 0 to 1) and from 1.113 to 0 μ_B (from x = 1 to 2), further demonstrating the cationic double redox of $Ni^{2+}(t_{2g}^6e_g^2)$/$Ni^{4+}(t_{2g}^6e_g^0)$ during the delithiation (Table S3). The magnetic moments of O almost remained at 0 μ_B during the delithiation process, indicating that Ni ions were the sole source of charge transfer.

Convex hulls, voltage profiles, and energy densities

Next, the ground-state Li/vacancy configurations and voltage profiles *vs.* Li concentrations of the three materials were studied (the details of the method are presented in S1). The convex hulls obtained from the formation energies, as well as corresponding averaged voltage profiles, are presented in Fig. 4a–c.

Regarding $Li_{(1-x)}NiO_2$, Fig. 4a shows that three stable intermediate ground states were predicted at x = 0.25, 0.5, and 0.75, and the corresponding Li/vacancy configurations without apparent lattice structural transformation are shown in Fig. S5a. The lattice volume of $Li_{(1-x)}NiO_2$ shrunk by ~8% after full delithiation (Fig. S6). The $LiNiO_2$ cathode material exhibited an averaged potential window of 3.3–4.3 V (Fig. 4a), which is consistent with the reported experimental and theoretical results [8,39]. Regarding $Li_{(2-x)}NiO_2$, two stable intermediate ground states were predicted at x = 0.5 and 1, and the corresponding Li/vacancy configurations are depicted in Fig. S5b. The Li ions

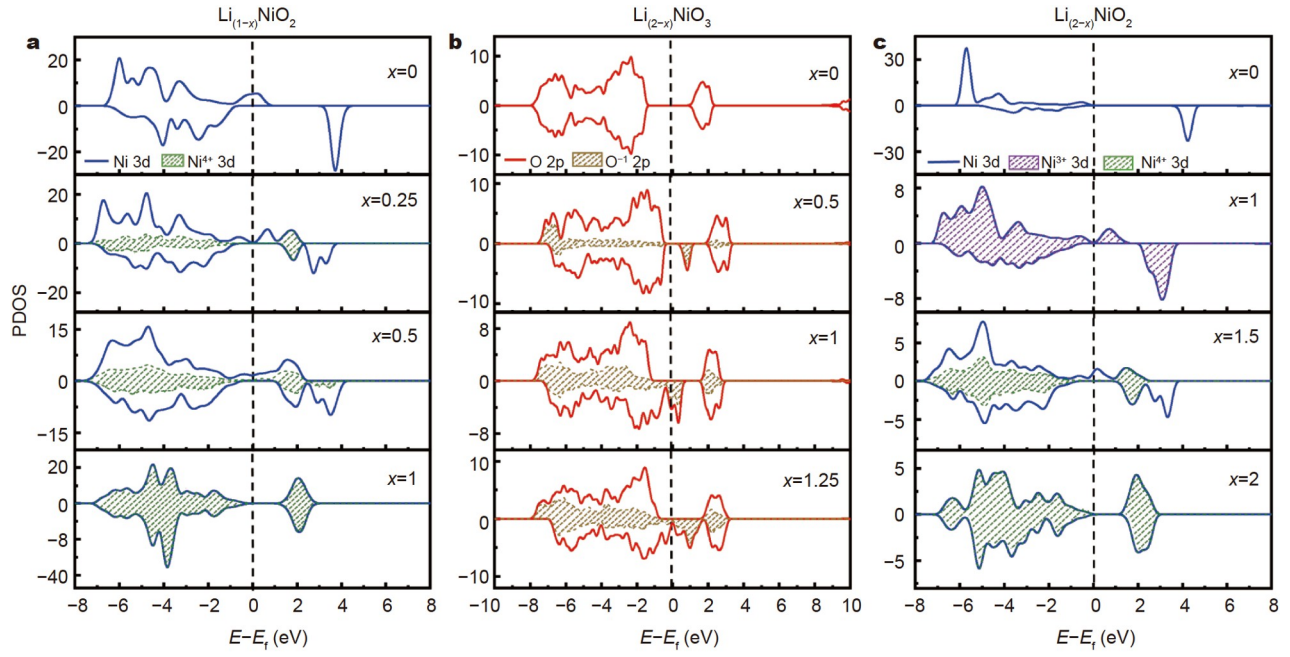

Figure 3 Projected DOS (PDOS) of the Ni-3d (blue lines) and O-2p (red lines) orbitals in $Li_{(1-x)}NiO_2$, $Li_{(2-x)}NiO_3$, and $Li_{(2-x)}NiO_2$, respectively. The dashed area indicates the PDOS of the oxidized ions.

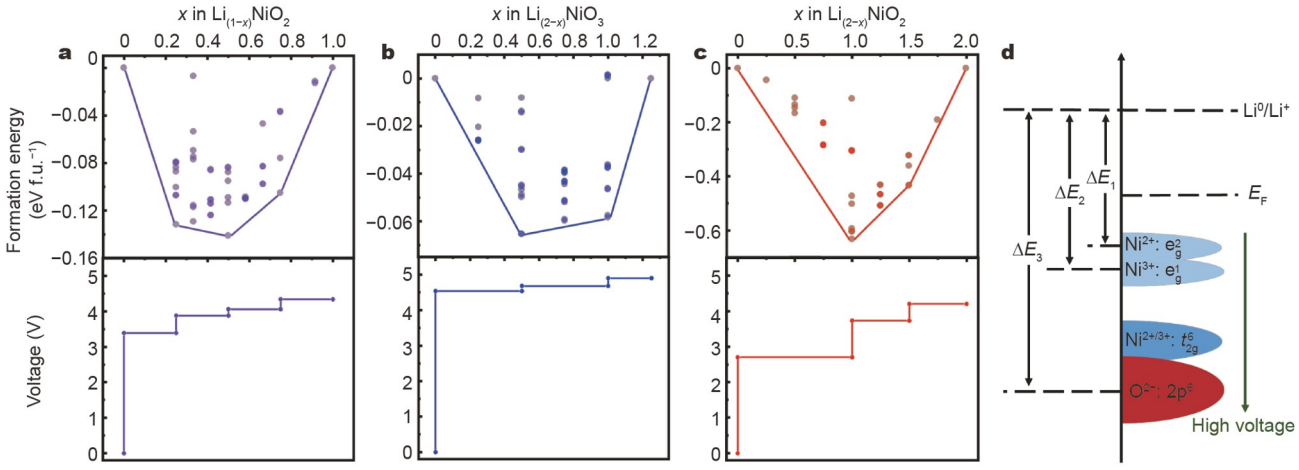

Figure 4 Formation energies of the ground-state configurations, convex hull, and average voltage profiles of (a) $LiNiO_2$, (b) Li_2NiO_3, and (c) Li_2NiO_2. (d) Schematic of the electronic structure. ΔE is the energy gap between the energy level of the electrons participating in the redox reaction and the Li^+/Li^0 energy level.

preferred to be removed from the 4h sites at $x = 0.5$ and the 4h and 2c sites at lowered Li ion concentrations ($x = 1$), indicating that the Li ions in the 4h sites would be extracted first during delithiation. The volume of the $Li_{(2-x)}NiO_3$ lattice first increased with $x < 1$ before decreasing with $x > 1$ (Fig. S6), and the degree of the volume reduction did not exceed 2.5% during delithiation ($0.0 < x < 1.25$). At $x > 1.25$, the appearance of the O dimers induced structural transformation with serious volume change. Additionally, the Li_2NiO_3 cathode exhibited an averaged potential window of 4.5–4.9 V with slight differences between the three voltage plateaus (Fig. 4b). Regarding $Li_{(2-x)}NiO_2$, two stable intermediate ground states were predicted at $x = 0.5$ and 1 (Fig. 4c), and the corresponding Li/vacancy configurations are shown in Fig. S5c. At $x = 1$ (with the composition of $LiNiO_2$), the structure exhibited the $C2/m$ phase with a collaborative Jahn–Teller distortion that was different from the $R\bar{3}m$ phase of the synthesized $LiNiO_2$. Fig. S6 shows that $Li_{(2-x)}NiO_2$ exhibited a large volume shrink (by ~25%) after full delithiation ($x = 0$–2); this was mainly facilitated by the first half-round of delithiation (~20% drastic volume shrink from $x = 0$ to 1). This large volume shrink was mainly due to the shrinking of the c-axis after the extraction of one layer of Li ions and the shrinking of the TM layers with a reduced Ni–O bond length after the oxidation of Ni^{2+} into Ni^{3+}. The Li_2NiO_2 cathode material exhibited an averaged potential window of 2.7–4.2 V, which is consistent with previous experimental results [8]. At the initial delithiation stage ($0 < x < 1$), the voltage plateau increased to 2.7 V, and an evident two-phase transition process occurred from 1T-Li_2NiO_2 to $C2/m$ $LiNiO_2$.

The operating voltages of the electrodes were primarily

determined by the local electronic structure and states of the electrons that participated in the redox reaction (irrespective of the TM 3d-electrons or 2p-electrons of the anions) [40]. The 3d orbitals of TM generally overlap with the 2p orbitals of O, forming TM–O bonds with particular ionic and covalent characteristics that are determined by the types of metals and anions, as well as the crystal structure. From the crystal-field theory, the Ni and O atoms displayed octahedral coordination (a NiO_6 octahedral structure) in those three materials, and the energy levels of the five 3d orbitals of the Ni ions were split into a high energy, e_g ($d_{x^2-y^2}$ and d_{z^2}), and low energy, t_{2g} orbitals (d_{xy}, d_{yz}, and d_{xz}). Considering the possible redox couples of $Ni^{2+}(t_{2g}^6e_g^2)$/$Ni^{3+}(t_{2g}^6e_g^1)$, $Ni^{3+}(t_{2g}^6e_g^1)$/$Ni^{4+}(t_{2g}^6e_g^0)$, and $O^{2-}(2p^6)$/$O^{1-}(2p^5)$, the transfer of electrons only involved the outer e_g level for the Ni ions and the 2p orbital electrons of the O ions. Consequently, the energy (ΔE), which was required to remove an electron that was participating in the redox reaction from its energy level to the Li^+/Li^0 energy level, determines the redox potentials [41]. Fig. 4d schematically shows that ΔE varied with different valences and elements. Therefore, the energy (ΔE_3) required to remove an electron from the O-2p levels was significantly larger than that required to remove an electron from the e_g levels of the octahedrally coordinated Ni ions (ΔE_1 or ΔE_2). Thus, Li_2NiO_3 with sequent O redox exhibited the highest redox potential among the three materials. The Ni^{3+}/Ni^{4+} monoelectron cationic redox occurred in $LiNiO_2$, and the Ni^{2+}/Ni^{4+} double-electron redox was observed in Li_2NiO_2. The energy of the Ni^{2+}/Ni^{3+} redox couple (ΔE_1) was smaller than that of the Ni^{3+}/Ni^{4+} redox couple (ΔE_2). Thus, $LiNiO_2$ exhibited higher voltage profiles than Li_2NiO_2 at the initial delithiation stage; they exhibited similar potentials after the oxidation of Ni^{2+} into Ni^{3+} in Li_2NiO_2.

The theoretical energy densities can be estimated based on the redox potentials and theoretical specific capacities (see details in S1). The theoretical specific capacity of $LiNiO_2$ was 274.45 mA h g^{-1}. Compared with $LiNiO_2$, although excess Li ions could be stored in Li_2NiO_3, only 62.5% of Li ions (1.25 Li per formula) could be extracted during electrochemical cycling. The remaining Li ions could not be extracted owing to the appearance of the O dimers and rapid phase transition. Thus, the theoretical specific capacity of Li_2NiO_3 was 277.78 mA h g^{-1}, indicating almost no improvement in the capacity compared with $LiNiO_2$. Contrarily, Li_2NiO_2 exhibited impressive improvement, achieving the highest theoretical specific capacity (512.46 mA h g^{-1}) owing to the double-redox activity. Although $LiNiO_2$ and Li_2NiO_3 exhibited approximate theoretical specific capacities, the theoretical energy density of Li_2NiO_3 (1297.11 W h kg^{-1}) was 26% larger than that of $LiNiO_2$ (1074.95 W h kg^{-1}) owing to the higher potential of Li_2NiO_3 with the anionic redox. Particularly, the double-redox activity endowed Li_2NiO_2 with the highest theoretical energy density (1708.94 W h kg^{-1}), which represented a great improvement over $LiNiO_2$ and Li_2NiO_3.

Oxygen thermal stability

Finally, since improved thermal stability and rapid oxygen release are required in cathode materials for high energy and power density applications in EV LIBs, the oxygen thermal stabilities of the three materials were also considered. Fig. 5a shows a comparison between the variations in the O-vacancy formation energy *vs.* delithiations of $LiNiO_2$ (purple line), Li_2NiO_3 (blue line), and Li_2NiO_2 (red line) (see details in S1). It was observed that all the materials tended to form O vacancies after delithiation since the vacancy formation energies were lowered in their delithiated states. The original Li_2NiO_3 exhibited the smallest vacancy formation energy among the three materials, and the negative O-vacancy formation energies of delithiated Li_2NiO_3 indicated that the formation of the O-vacancy was thermodynamically favorable. The vacancy formation energies of $LiNiO_2$ were much smaller than that of Li_2NiO_2 in the initial delithiation state and similar to that of Li_2NiO_2, following further delithiation because Li_2NiO_2 was converted into *C*2/*m* $LiNiO_2$ after half extraction of the Li-ion layer, which permitted the double-electron cationic charge-transfer process and prevented the compound from utilizing the oxygen redox to trigger oxygen loss. Therefore, Li_2NiO_2 exhibited the best oxygen thermal stability.

DISCUSSION

Fig. 5b shows an all-around comparison of the above results obtained for $LiNiO_2$ (purple line), Li_2NiO_3 (blue line), and

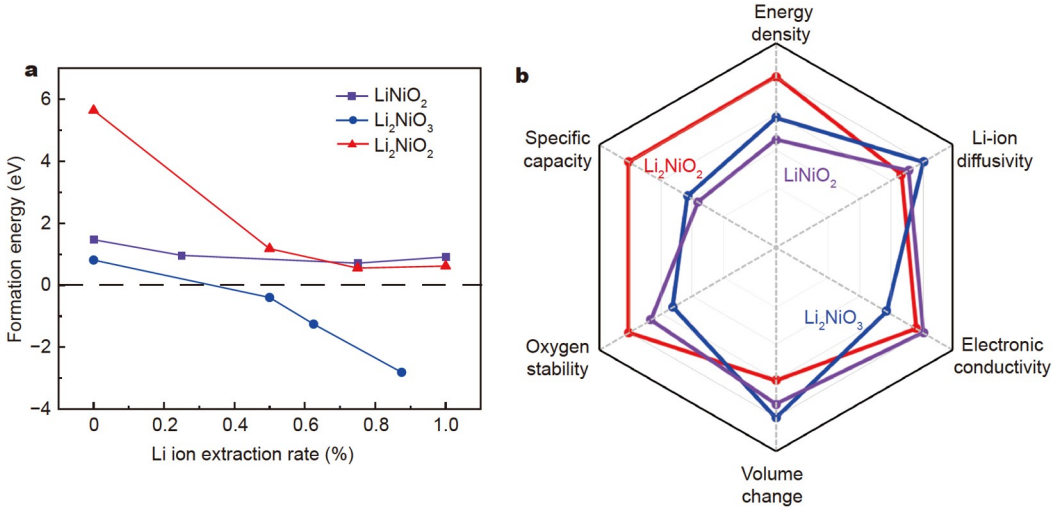

Figure 5 (a) Evolution of the O-vacancy formation energies of $LiNiO_2$ (purple line), Li_2NiO_3 (blue line), and Li_2NiO_2 (red line) upon delithiation. (b) Radar plot of the all-around comparison of the properties of $LiNiO_2$ (purple line), Li_2NiO_3 (blue line), and Li_2NiO_2 (red line) as cathodes.

Li_2NiO_2 (red line). Owing to the existence of the $[Li_{1/3}Ni_{2/3}]O_2$ layers, Li_2NiO_3 exhibited the best Li-ion diffusivity, as well as the least volume change (only 2.5% at $x < 1.25$) during delithiation, although it suffered from poor oxygen thermal stability owing to the anionic redox activity and poor electronic conductivity, which were induced by the 2.03-eV bandgap and the formation of polarons following delithiation. Since an additional Li layer would reduce the open space for Li diffusion, the diffusivity of the Li ions in Li_2NiO_2 was more challenging at the initial delithiation stage than at other stages (details on the diffusivity are presented in S3), although it became easier as more Li ions were extracted. Although Li_2NiO_2 is a semiconductor exhibiting a large bandgap (3.66 eV), the insulator-metal transition occurred immediately, following the slight extraction of Li-ion. Thus, the excess Li ions in Li_2NiO_2 lowered the valence state of Ni ions to the lowest state, Ni^{2+}, resulting in the best oxygen thermal stability, as well as a slightly lower early redox potential. Li_2NiO_2 exhibited a reversible Ni^{2+}/Ni^{4+} double redox and an impressive energy density value (1708.94 W h kg^{-1}). Thus, the absolute advantages (capacity, energy density, electronic conductivity, and thermal stability) of Li_2NiO_2 as cathodes for LIBs owing to the Ni^{2+}/Ni^{4+} double redox rendered it the most promising candidate for next-generation layered oxide cathodes. However, Li_2NiO_2 suffered great volume reduction (by ~25%), which was its only disadvantage. This would damage its cycling stability (Fig. S6). Great efforts must be invested in developing Li_2NiO_2-based cathodes in the future.

Here, we proposed two approaches for reducing the volume change in Li_2NiO_2 during delithiation. One of the approaches involved the insertion of large-radius ions into the Li slab to reduce the shrinking of the *c*-axis; the other approach involved doping in Ni layers to reduce the shrinking of TM layers. For example, we calculated the volume evolution of partial Na-ions that were inserted in the Li slab ($Li_2Na_{0.25}NiO_2$) and Mo ions substituting the half Ni ions ($Li_2Ni_{0.5}Mo_{0.5}O_2$) (Fig. S7), and the structure evolutions of $Li_2Na_{0.25}NiO_2$ and $Li_2Ni_{0.5}Mo_{0.5}O_2$ are shown in Fig. S8. The volume-reduction rate with delithiation decreased sequentially from 25% to 16% in $Li_2Na_{0.25}NiO_2$. Regarding $Li_2Ni_{0.5}Mo_{0.5}O_2$, the volume shrank by 10% after the extraction of one layer of Li ions (from $x = 0$ to 1), while the volume expanded by 1% during the second half delithiation (from $x = 1$ to 2), resulting in a total volume-reduction rate of 9% after full delithiation.

CONCLUSION

In summary, we selected typical reversible Li_2NiO_3 and 1T-Li_2NiO_2 as two representative materials for developing next-generation layered TM oxide cathodes to break the $LiNiO_2$ limit, after which we comprehensively compared them with $LiNiO_2$ regarding their overall properties as cathodes from a theoretical perspective. Owing to the cationic double-redox activity, Li_2NiO_2 exhibited several absolute advantages regarding the capacity, energy density, electronic conductivity, and thermal stability over the other materials as cathodes for LIBs, revealing that the cationic M^{2+}/M^{4+} double redox (M denotes a TM) is a promising material beyond the M^{3+}/M^{4+} mono redox or anionic redox for next-generation layered oxide cathodes with high-energy-density and oxygen stability. The high throughput screening approach based on *ab initio* calculations or machine learning methods could be employed to develop or design new cathode materials with multiple cationic redox to develop next-generation alternative lithium-ion cathode materials.

Received 16 July 2021; accepted 13 October 2021; published online 22 November 2021

1 Kuo LY, Guillon O, Kaghazchi P. On the origin of non-monotonic variation of the lattice parameters of $LiNi_{1/3}Co_{1/3}Mn_{1/3}O_2$ with lithiation/delithiation: a first-principles study. J Mater Chem A, 2020, 8: 13832–13841
2 Choi J, Manthiram A. Role of chemical and structural stabilities on the electrochemical properties of layered $LiNi_{1/3}Mn_{1/3}Co_{1/3}O_2$ cathodes. J Electrochem Soc, 2005, 152: A1714
3 Lee E, Persson KA. Structural and chemical evolution of the layered Li-excess Li_xMnO_3 as a function of Li content from first-principles calculations. Adv Energy Mater, 2014, 4: 1400498
4 Marusczyk A, Albina JM, Hammerschmidt T, *et al.* Oxygen activity and peroxide formation as charge compensation mechanisms in Li_2MnO_3. J Mater Chem A, 2017, 5: 15183–15190
5 Jiao C, Xu G, Wang M, *et al.* Improving electrochemical performance of Li-rich cathode materials *via* adjusting the components. Solid State Ion, 2021, 369: 115722
6 Ramos-Sanchez G, Romero-Ibarra IC, Vazquez-Arenas J, *et al.* Controlling Li_2CuO_2 single phase transition to preserve cathode capacity and cyclability in Li-ion batteries. Solid State Ion, 2017, 303: 89–96
7 Dahn J. Structure and electrochemistry of $Li_{1\pm y}NiO_2$ and a new Li_2NiO_2 phase with the $Ni(OH)_2$ structure. Solid State Ion, 1990, 44: 87–97
8 Kang K, Chen CH, Hwang BJ, *et al.* Synthesis, electrochemical properties, and phase stability of Li_2NiO_2 with the *Immm* structure. Chem Mater, 2004, 16: 2685–2690
9 Lin CJ, Zheng F, Zhu ZZ. Electronic structures and Li diffusion in cathode material Li_2FeO_2 of Li-ion batteries. Acta Phys Sin, 2019, 68: 157201
10 Wu Z, Ji S, Zheng J, *et al.* Prelithiation activates $Li(Ni_{0.5}Mn_{0.3}Co_{0.2})O_2$ for high capacity and excellent cycling stability. Nano Lett, 2015, 15: 5590–5596
11 Love CT, Dmowski W, Johannes MD, *et al.* Structural originations of irreversible capacity loss from highly lithiated copper oxides. J Solid State Chem, 2011, 184: 2412–2419
12 Aguilar-Eseiza N, Ramos-Sánchez G, González F, *et al.* High voltage-improved reversible capacity in $Ni^{+2/+3}$ modified copper-based cathodes for lithium ion batteries. Electrochem Commun, 2018, 96: 32–36
13 Martínez-Cruz MA, Yañez-Aulestia A, Ramos-Sánchez G, *et al.* Unraveling the effects on lithium-ion cathode performance by cation doping M–Li_2CuO_2 solid solution samples (M = Mn, Fe and Ni). Dalton Trans, 2020, 49: 4549–4558
14 Arachi Y, Ide T, Nakagawa T, *et al.* Crystal structures and electrochemical properties of Ni-substituted Li_2CuO_2 as a cathode material. ECS Trans, 2013, 50: 143–151
15 Kordatos A, Kuganathan N, Kelaidis N, *et al.* Defects and lithium migration in Li_2CuO_2. Sci Rep, 2018, 8: 7
16 Ruther RE, Samuthira Pandian A, Yan P, *et al.* Structural transformations in high-capacity $Li_2Cu_{0.5}Ni_{0.5}O_2$ cathodes. Chem Mater, 2017, 29: 2997–3005
17 Lee H, Chang SK, Goh EY, *et al.* Li_2NiO_2 as a novel cathode additive for overdischarge protection of Li-ion batteries. Chem Mater, 2008, 20: 5–7
18 Park H, Yoon T, Kim YU, *et al.* Li_2NiO_2 as a sacrificing positive additive for lithium-ion batteries. Electrochim Acta, 2013, 108: 591–595
19 Johnson CS, Kim JS, Kropf AJ, *et al.* Structural characterization of layered $Li_xNi_{0.5}Mn_{0.5}O_2$ ($0 < x \leq 2$) oxide electrodes for Li batteries. Chem Mater, 2003, 15: 2313–2322
20 Perdew JP, Chevary JA, Vosko SH, *et al.* Atoms, molecules, solids, and surfaces: Applications of the generalized gradient approximation for exchange and correlation. Phys Rev B, 1992, 46: 6671–6687
21 Ong SP, Hautier G., Kocher M, *et al.* The materials project (https://www.Materialsproject.Org/)
22 Bianchini M, Roca-Ayats M, Hartmann P, *et al.* There and back again—The journey of $LiNiO_2$ as a cathode active material. Angew Chem Int Ed, 2019, 58: 10434–10458
23 Dyer LD, Borie Jr. BS, Smith GP. Alkali metal-nickel oxides of the type

$MNiO_2$. J Am Chem Soc, 1954, 76: 1499–1503
24 Migeon HN, Zanne M, Gleitzer C, *et al.* The Li_2O-NiO-O_2 system at 670°C and the consequences of non-stoichiometry on the magnetic properties of the $Li_xNi_{1-x}O_{1\pm y}$ phases. J Mater Sci, 1978, 13: 461–466
25 Shinova E, Zhecheva E, Stoyanova R, *et al.* High-pressure synthesis of solid solutions between trigonal $LiNiO_2$ and monoclinic $Li[Li_{1/3}Ni_{2/3}]O_2$. J Solid State Chem, 2005, 178: 1661–1669
26 Billerey D, Terrier C, Mainard R, *et al.* Magnetic-structure of $NiCl_2$ at 4.2 K by neutron-diffraction. Comptes Rendus Hebdomadaires Des Seances De L Acad Des Sci B, 1977, 284: 495–498
27 Momeni M, Yousefi Mashhour H, Kalantarian MM. New approaches to consider electrical properties, band gaps and rate capability of same-structured cathode materials using density of states diagrams: Layered oxides as a case study. J Alloys Compd, 2019, 787: 738–743
28 Molenda J. Structural, electrical and electrochemical properties of $LiNiO_2$. Solid State Ion, 2002, 146: 73–79
29 Zheng J, Ye Y, Pan F. 'Structure units' as material genes in cathode materials for lithium-ion batteries. Natl Sci Rev, 2020, 7: 242–245
30 Wang ZQ, Wu MS, Xu B, *et al.* Improving the electrical conductivity and structural stability of the Li_2MnO_3 cathode *via* P doping. J Alloys Compd, 2016, 658: 818–823
31 Ye YK, Hu ZX, Liu JH, *et al.* Research progress of theoretical studies on polarons in cathode materials of lithium-ion batteries. Acta Phys-Chim Sin, 2021, 37: 2011003
32 Bianchini M, Schiele A, Schweidler S, *et al.* From $LiNiO_2$ to Li_2NiO_3: Synthesis, structures and electrochemical mechanisms in Li-rich nickel oxides. Chem Mater, 2020, 32: 9211–9227
33 Marianetti CA, Kotliar G, Ceder G. A first-order Mott transition in Li_xCoO_2. Nat Mater, 2004, 3: 627–631
34 Jung R, Metzger M, Maglia F, *et al.* Oxygen release and its effect on the cycling stability of $LiNi_xMn_yCo_zO_2$ (NMC) cathode materials for Li-ion batteries. J Electrochem Soc, 2017, 164: A1361–A1377
35 Li N, Sallis S, Papp JK, *et al.* Unraveling the cationic and anionic redox reactions in a conventional layered oxide cathode. ACS Energy Lett, 2019, 4: 2836–2842
36 Sathiya M, Rousse G, Ramesha K, *et al.* Reversible anionic redox chemistry in high-capacity layered-oxide electrodes. Nat Mater, 2013, 12: 827–835
37 Zheng J, Teng G, Yang J, *et al.* Mechanism of exact transition between cationic and anionic redox activities in cathode material Li_2FeSiO_4. J Phys Chem Lett, 2018, 9: 6262–6268
38 Strehle B, Kleiner K, Jung R, *et al.* The role of oxygen release from Li- and Mn-rich layered oxides during the first cycles investigated by on-line electrochemical mass spectrometry. J Electrochem Soc, 2017, 164: A400–A406
39 Yan HJ, Li B, Jiang N, *et al.* First-principles study: The structural stability and sulfur anion redox of $Li_{1-x}Nio_{2-y}S_y$. Acta Phys-Chim Sin, 2017, 33: 1781–1788
40 Sun G, Yu FD, Que LF, *et al.* Local electronic structure modulation enhances operating voltage in Li-rich cathodes. Nano Energy, 2019, 66: 104102
41 Yao Z, Kim S, He J, *et al.* Interplay of cation and anion redox in $Li_4Mn_2O_5$ cathode material and prediction of improved $Li_4(Mn,M)_2O_5$ electrodes for Li-ion batteries. Sci Adv, 2018, 4: eaao6754

Acknowledgements This work was financially supported by the starting fund of Peking University, Shenzhen Graduate School and Fujian Science & Technology Innovation Laboratory for Energy Devices of China (21C-LAB).

Author contributions Jia Y, Pan F and Zheng J conceived the idea and designed the project. Jia Y performed all the calculations. Ye Y wrote the programs to process the data. Liu J, Zheng S, Lin W, Wang Z, and Li S analyzed the results and participated in the discussion of mechanism. Jia Y and Zheng J wrote the manuscript and all authors edited the manuscript.

Conflict of interest The authors declare that they have no conflict of interest.

Supplementary information Details for the calculations and supporting data are available in the online version of the paper.

Yining Jia is a master student at the School of Advanced Materials, Peking University, Shenzhen Graduate School. Her research focuses on computational materials and energy materials.

Feng Pan is Chair-Professor, Founding Dean of the School of Advanced Materials, Peking University, Shenzhen Graduate School. He received his PhD degree from the Department of P&A Chemistry, University of Strathclyde, Glasgow, U.K., receiving the "Patrick D. Ritchie Prize" for the best PhD in 1994. Prof. Pan has been engaged in fundamental research and product development of novel optoelectronic and energy storage materials and devices.

Jiaxin Zheng received his PhD degree in condensed physics from Peking University in 2013. He is currently working at the School of Advanced Materials, Peking University as an Associate Professor. His research interests include computational materials and energy materials.

打破$LiNiO_2$的能量密度极限: Li_2NiO_3还是Li_2NiO_2?

贾怡宁[1], 叶耀坤[1], 刘佳华[1], 郑世胜[1], 林伟成[1], 王竹[1], 李舜宁[1], 潘锋[1*], 郑家新[1,2*]

摘要 开发新一代层状氧化物阴极, 是发展高能量密度电动汽车锂离子电池迫切关注的问题. 目前有一种方法是不断提高镍基层状氧化物中的镍含量, 但这一方法的极限是$LiNiO_2$. 为了突破这一极限, 获得更高的能量密度, 近年来备受关注的一种方法是在过渡金属层中引入过量的锂离子, 形成Li_2MO_3 (M是过渡金属阳离子). 然而, 还有一种一直被忽视的方法是在过渡金属层和原始Li层之间插入一层额外的Li离子, 形成Li_2MO_2. 本研究中, 我们选择了典型的Li_2NiO_3和1T-Li_2NiO_2作为代表, 从理论角度综合比较了Li_2NiO_3、1T-Li_2NiO_2和$LiNiO_2$的各项电化学性能. 我们发现, 不同于$LiNiO_2$中发生的Ni^{3+}/Ni^{4+}单电子阳离子氧化还原, 在Li_2NiO_3中存在着伴有极化子的阴离子氧化还原. 而在Li_2NiO_2中, 则发生了伴有绝缘体到金属转变的Ni^{2+}/Ni^{4+}双电子氧化还原. 在这三种材料中, 由于Li_2NiO_2具有双电子氧化还原活性, 其在容量、能量密度、电导率和热稳定性等方面都表现优异, 是最有希望突破$LiNiO_2$极限的下一代层状氧化物阴极材料. 虽然Li_2NiO_2具有脱锂过程中的体积变化较大的缺点, 但我们提出了两种可能的解决方法: 在Li层中掺杂Na和在TM层中掺杂Mo, 都获得了不错的效果. 这一工作为如何突破$LiNiO_2$的能量密度极限, 开发下一代具有高能量密度的层状氧化物阴极提供了新的思路.

